

High Osteogenic Potential of Adipose- and Muscle-derived Mesenchymal Stem Cells in Spinal-Ossification Model Mice

Xizhe Liu, MD,* Gentaro Kumagai, MD, PhD,* Kanichiro Wada, MD, PhD,* Toshihiro Tanaka, MD, PhD,* Toru Asari, MD, PhD,* Kazuki Oishi, MD, PhD,* Taku Fujita, MD,* Hiroki Mizukami, MD, PhD,[†] Ken-Ichi Furukawa, PhD,[‡] and Yasuyuki Ishibashi, MD, PhD*

Study Design. Basic experiments in a mouse model of ossification of the posterior longitudinal ligament (OPLL).

Objective. To assess the osteogenic potential of mesenchymal stem cells (MSCs) obtained from muscle and adipose tissue in Tiptoe-walking (*ttw*) mice, in which cervical OPLL compresses the spinal cord and causes motor and sensory dysfunction.

Summary of Background Data. In humans, MSCs have been implicated in the pathogenesis of cervical OPLL. Cervical OPLL in *ttw* mice causes chronic compression of the spinal cord. Few studies have compared the MSC osteogenic potential with behavioral changes in an OPLL animal model.

Methods. We compared the osteogenic potential and behavioral characteristics of MSCs from *ttw* mice (4 to 20 weeks old) with those from control wild-type mice (without hyperostosis). Ligament ossification was monitored by micro-computed tomography and pathology; tissues were double stained with fluorescent antibodies against markers for MSCs (CD45 and CD105), at

From the *Department of Orthopedic Surgery, Hirosaki University Graduate School of Medicine, Hirosaki, Aomori, Japan; [†]Department of Pathology and Molecular Medicine, Hirosaki University Graduate School of Medicine, Hirosaki, Aomori, Japan; and [‡]Department of Pharmacology, Hirosaki University Graduate School of Medicine, Hirosaki, Aomori, Japan.

Acknowledgment date: January 27, 2017. First revision date: March 29, 2017. Second revision date: April 11, 2017. Acceptance date: May 4, 2017.

The manuscript submitted does not contain information about medical device(s)/drug(s).

AOSpine Japan Research Grant 2016 (101278); the Public Health Bureau of the Japanese Ministry of Labour, Health, and Welfare; and a Grant-in-Aid from the Ministry of Education, Culture, Sports, Science, and Technology of Japan (24590310) funds were received in support of this work.

No relevant financial activities outside the submitted work.

This is an open access article distributed under the terms of the Creative Commons Attribution-Non Commercial-No Derivatives License 4.0 (CCBY-NC-ND), where it is permissible to download and share the work provided it is properly cited. The work cannot be changed in any way or used commercially without permission from the journal.

Address correspondence and reprint requests to Gentaro Kumagai, MD, PhD, Department of Orthopedic Surgery, Hirosaki University Graduate School of Medicine, Hirosaki University, Hirosaki, Aomori 036-8562, Japan; E-mail: gen722@hirosaki-u.ac.jp

DOI: 10.1097/BRS.0000000000002266

E1342 www.spinejournal.com

8 weeks. The Basso Mouse Scale was used to assess motor function, and heat and mechanical tests to assess sensory function. The osteogenic potential of adipose and muscle MSCs was assessed by Alizarin Red S absorbance, staining for osteogenic mineralization, and real-time quantitative polymerase chain reaction for osteogenesis-related genes.

Results. Spinal-ligament ossification began in *ttw* mice at 8 weeks of age, and the ossified area increased with age. Immunofluorescence staining identified MSCs in the ossification area. The *ttw* mice became hyposensitive at 8 weeks of age, and Basso Mouse Scale scores showed motor-function deficits starting at 12 weeks of age. Alizarin Red S staining for mineralization showed a higher osteogenic potential in the adipose- and muscle-derived MSCs from *ttw* mice than from wild-type mice at 4, 8, and 20 weeks of age. Real-time quantitative polymerase chain reaction showed that *ttw* MSCs strongly expressed osteogenesis-related genes.

Conclusion. MSCs derived from muscle and adipose tissue in *ttw* mice had a high osteogenic potential.

Key words: cell differentiation, mesenchymal stem cells, ossification of the posterior longitudinal ligament, osteogenesis, *ttw* mice.

Level of Evidence: N/A

Spine 2017;42:E1342–E1349

Ossification of the posterior longitudinal ligament (OPLL) of the cervical spine is a common musculoskeletal disease.¹ Risk factors associated with OPLL development and progression include diabetes mellitus and genetic, hormonal, environmental, and lifestyle factors.^{2,3} The pathogenesis of OPLL is unclear.

Human mesenchymal stem cells (MSCs) have been isolated from various tissues. Although MSCs are thought to supply essential progenitor cells for repairing damaged tissues,^{4,5} MSCs also contribute to pathogenic conditions such as fibrodysplasia ossificans progressiva,⁶ ectopic ossification after burn injury,⁷ and aortic valve calcification.⁸ MSCs are putative stem/progenitor cells in trauma-induced

heterotopic ossification of the extremities.⁹ We previously demonstrated that MSCs are present in and can be isolated from ossified spinal ligaments in humans.^{10,11} These MSCs have a higher ossification potential than those from non-ossified ligaments.¹² However, samples from humans can vary with age, sex, main syndrome, complications, and the type of OPLL, so it is essential to characterize MSCs in an OPLL animal model.

Mutant spinal hyperostotic *ttw* mice, known as Tiptoe-walking mice, are a model for progressive ectopic ossification.¹³ *Ttw* mice develop progressive abnormal ossification and calcification primarily of the cartilage and tendons of the spine and limbs, and suffer from severe deformation and ankylosis. Ligament ossification compresses the spinal cord, diminishing motor function over time, as shown by diffusion tensor tractography.¹⁴ However, how OPLL-related spinal-cord compression changes sensory function, including cutaneous sensitivity to mechanical stimuli and heat, is unclear.

The present study assessed the osteogenic potential of MSCs from muscle and adipose tissue in *ttw* mice, which have motor and sensory deficits due to OPLL-related spinal cord compression.

MATERIALS AND METHODS

Study Design

All experiments were performed according to the Guidelines for Animals of the Graduate School of Hirosaki University and the Central Institute for Experimental Animals. Approval for the present study was obtained from the Committee on the Ethics of Animal Experimentation of Hirosaki University. Male C57BL6 mice (CLEA Japan, Inc, Tokyo, Japan) were used as wild-type (WT) control mice. To generate the mouse spinal ligament ossification model, Institute of Cancer Research mice were obtained from the Central Institute for Experimental Animals (Kawasaki, Japan), and siblings were mated to produce *ttw* mice. Male *ttw* mice were used in the experiments.

Micro-computed Tomography

To observe the process of OPLL, all samples were examined by micro-computed tomography (micro-CT; Scan X-mate-L090, Comscantecno, Yokohama, Japan) before slicing with the source at 75 kVp and 100 mA and the specimen positioned for a magnification of 4.657. Micro-CT images were obtained of samples obtained from *ttw* mice every 4 weeks from 4 to 20 weeks of age.

Histological Analysis

WT and *ttw* mice were euthanized by anesthesia overdose for histological analysis at regular intervals beginning at 8 weeks of age, and the spines were dissected and fixed with 70% ethanol. The specimens were decalcified with KC-X solution (Falma, Tokyo, Japan), embedded in paraffin, and sliced into 10- μ m-thick sections. The samples were screened by hematoxylin and eosin staining, and then stained with toluidine blue for chondrocytes. Samples were then

double-stained with tartrate-resistant acid phosphatase (TRAP) for osteoclasts and alkaline phosphatase (ALP) for osteoblasts. Whole areas of each section were captured with a digital microscope system (BZ-X700, Keyence, Osaka, Japan) for morphological assessment.

Immunofluorescence Cell Staining

Samples from 8-week-old mice were double-stained with fluorescent antibodies for immunohistochemical analysis. The sections were washed with phosphate buffered saline (PBS) containing 0.01% Tween 20 (PBS-T) and treated with 1% bovine serum albumin (Sigma-Aldrich, MO) diluted in PBS.¹⁵ The samples were then incubated overnight at 4°C with a diluted mixture of two primary antibodies, monoclonal anti-CD44 conjugated with AF488, and monoclonal anti-CD105 conjugated with AF700 (Novusbio, Littleton, CO; rat), to detect MSC markers. The samples were stained with Hoechst (Thermo Scientific, Tokyo, Japan) for 15 minutes and examined with a fluorescence microscope (BZ-X700, Keyence).

Behavioral Assessment

All animals were tested for hindlimb motor function and mechanosensitivity every 4 weeks until 20 weeks of age ($n = 5$ at each time point). Two nonbiased observers analyzed hindlimb performance using the Basso Mouse Scale (BMS) locomotor rating scale.¹⁶ We also evaluated cutaneous sensitivity to mechanical stimuli and heat. In the heat test, hindpaw withdrawal from the glass floor of the chamber stopped the emitter and timer. The withdrawal latency was defined as the duration between the activation and termination of the infrared stimulus (measured in seconds); the final withdrawal latency was recorded as the mean of three measurements. After the latency measurement, the mice were placed in Plexiglass containers resting on an elevated wire mesh. Hindpaw withdrawal thresholds (measured at 5 g) in response to an innocuous mechanical stimulus were measured using a Dynamic Plantar Aesthesiometer.¹⁷ A plantar test was used to assess reactions to heat. In this test, mice were placed in Plexiglass containers resting on an elevated glass surface. A mobile infrared emitter below the glass was placed under the center of the mouse's plantar hindpaw, and activating the emitter started a timer.¹⁸

Mesenchymal Stem Cell Culture

WT and *ttw* adipose and muscle tissues were dissected from unossified samples of the inguinal and femur muscle attachment. The samples were minced into 0.5-mm³ pieces and washed with PBS. The pieces were digested with 3% type I collagenase (Wako Pure Chemical Industries, Osaka, Japan) at 37°C for 40 minutes (adipose tissue) or 60 minutes (muscle). The resultant cell suspension was filtered through a 70-mm mesh (BD Biosciences, San Jose, CA) to remove tissue debris and was centrifuged. The cells were resuspended in lysing buffer (BD Pharmaceutical Tokyo, Japan) following the manufacturer's protocol to remove red blood cells. Cells were cultured at 37°C with 5% CO₂ in culture medium consisting

TABLE 1. List of Primers for Real-Time Quantitative Polymerase Chain Reaction

Gene	Forward Primer 5'-3'	Reverse Primer 5'-3'
<i>GAPDH</i>	TGCACCACCAACTGCTTAG	GGATGCAGGGATGATGTTC
Osteopontin	ACACTTTCCTCAATCGTCC	TGCCCTTCCGTTGTTGTCC
Osteocalcin	TCTGACAAAGCCTTCATGTCC	AAATAGTGATACCGTAGATGCC
<i>RUNX2</i>	AGGGACTATGGCGTCAAACA	GGCTCACGTCGCTCATCTT
<i>BMP2</i>	TCAGAACACAAGTCAGTGGGA	TGGGTTCTCCTCTAAATGGGC
<i>ALP</i>	AACCCAGACACAAGCATTC	GAGACATTTCCCGTTCACC

ALP indicates alkaline phosphatase; *BMP2*, bone morphogenetic protein 2; *GAPDH*, glyceraldehyde-3-phosphate dehydrogenase; *RUNX2*, runt-related transcription factor 2.

of alpha minimum essential medium (Invitrogen, Carlsbad, CA) with 10% fetal bovine serum, 100 U/mL penicillin G sodium, and streptomycin sulfate (Invitrogen).^{19,20}

Flow Cytometry

To determine the phenotype of MSCs isolated and cultured from the target areas, the cells were counted and stained with rat antimouse CD34, CD45, and CD105 monoclonal antibodies (eBioscience, San Diego, CA). Alexa Fluor 647-, PE-Cy7-, and PE-conjugated antibodies were used as the antibody-binding dyes. Cell fluorescence was evaluated by flow cytometry using a fluorescence activated cell sorting (FACS Aria II) (BD Biosciences), and the data were analyzed with CellQuest software (BD Biosciences).

Mesenchymal Stem Cell Differentiation

Osteogenic Differentiation

Passage-3 adipose-derived MSCs (A-MSCs) and muscle-derived MSCs (M-MSCs) were plated at 4×10^4 cells/35 mm for cytohistological staining according to the manufacturer's instructions and cultured for 3 weeks in osteogenic-condition medium (PT3002, Lonza, Allendale, NJ). The cultures were rinsed with PBS and fixed with 10% formaldehyde, and matrix mineralization was visualized by 1% Alizarin Red S (Sigma-Aldrich, Tokyo, Japan). To quantify the induced mineralization, the bound stain was dissolved in cetylpyridinium chloride monohydrate (Wako Pure Chemical Industries) and measured at an optical density of 550 nm.²¹

Adipogenic Differentiation

Passage-3 A-MSCs and M-MSCs were plated at 1×10^5 cells/35-mm-diameter dish. The culture medium was replaced with conditioned medium as described in the manufacturer's protocol (PT3004, Lonza). After 21 days, the cultures were rinsed with PBS and fixed with 4% formaldehyde for 5 minutes, and lipid droplets were stained with Oil Red O (Wako Pure Chemical Industries).

Chondrogenic Differentiation

Passage-3 A-MSCs and M-MSCs (4×10^5 cells/pellet) were cultured in pellet form in the presence of inductive medium (PT3003, Lonza) as described in the manufacturer's protocol. For microscopy, the pellets were fixed in 10% formaldehyde, dehydrated through serial ethanol dilutions, embedded in

paraffin, cut into 5- μ m sections, and stained with toluidine blue (Kanto Chemical Co. Inc., Tokyo, Japan).

Real-Time Quantitative Polymerase Chain Reaction

Real-time quantitative polymerase chain reaction (qPCR) was used to detect the mRNA expression of the osteogenesis-related genes osteocalcin (*OCN*), osteopontin (*OPN*), bone morphogenetic protein 2 (*BMP2*), runt-related transcription factor 2 (*RUNX2*), and *ALP* in A-MSCs and M-MSCs after osteogenic induction in the 4th, 8th, and 20th weeks. Total RNA was extracted with the RNeasy Mini Kit (Qiagen, Valencia, CA) according to the manufacturer's protocol. Table 1 lists the PCR primers for osteogenesis-related genes; gene expression was normalized to that of glyceraldehyde-3-phosphate dehydrogenase.

Statistical Analysis

All data were expressed as the mean \pm SE. Experimental data were compared between groups by independent sample *t* test, and BMS scores were compared using paired *t* tests. FACS results were examined by two-way analysis of variance. A *P* value of <0.05 was considered statistically significant. Statistical calculations were performed with SPSS version 22.0 (SPSS, Chicago, IL).

RESULTS

Ligament Ossification Starts at 8 Weeks of Age in *ttw* Mice

To observe changes in OPLL in *ttw* mice, axial and sagittal micro-CT images were obtained at 4-week intervals from 4 to 20 weeks of age (Figure 1A). At 8 weeks of age, ossification was found near the posterior longitudinal ligament (PLL) originating from the atlantoaxial membrane. At 12 weeks, ossification appeared in the posterior longitudinal ligament and the anterior longitudinal ligament. At 16 weeks, the spinal cord was severely compressed at both the PLL and the yellow ligament. The ossified region at the center of the lesion continued to increase in size from 8 weeks of age onward.

Histological Analysis and Immunofluorescence Staining in the *ttw* Ossification Zone

Hematoxylin and eosin staining of the spine of 8-week-old *ttw* and WT mice revealed progressive ossification in the *ttw*

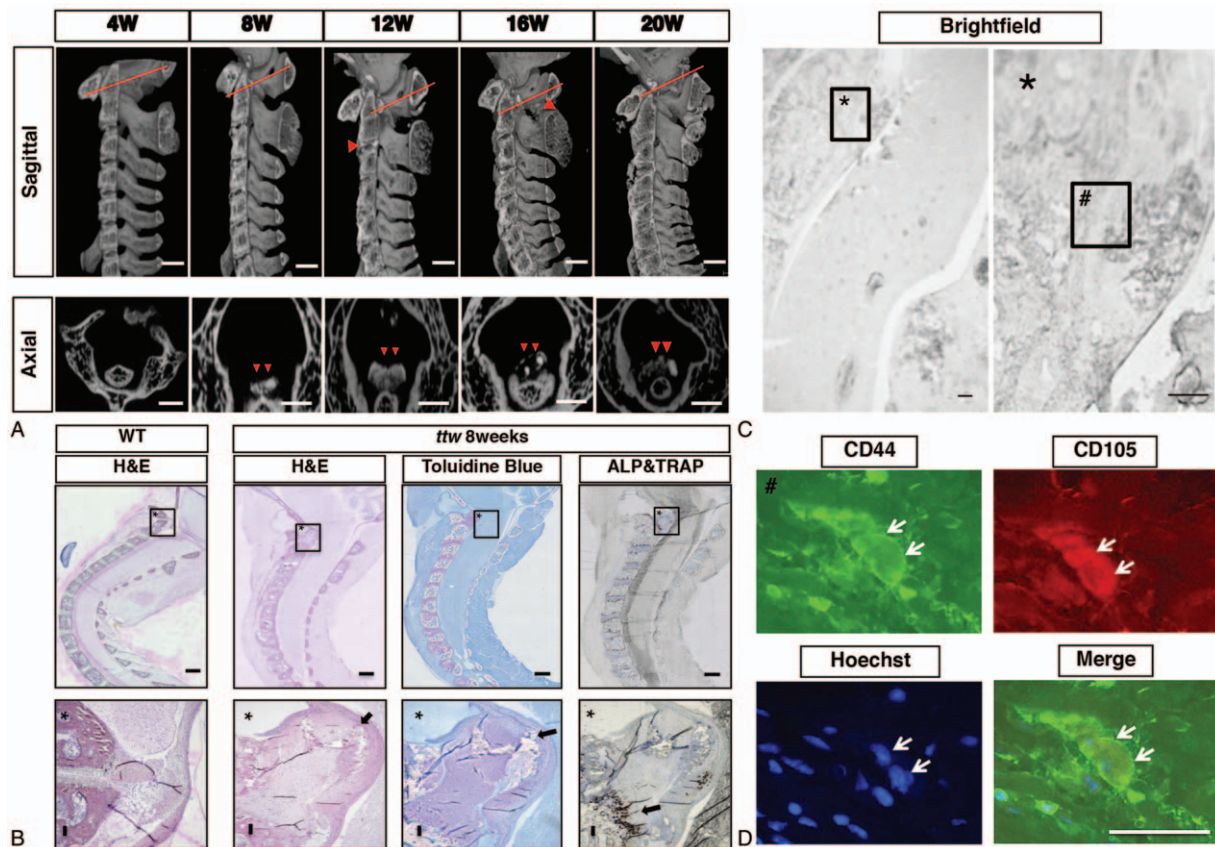


Figure 1. Ossification begins in 8-week-old *ttw* mice, with MSCs in the ossified lesion. **A**, Representative micro-computed tomography (CT) figures from *ttw* mice at 4 to 20 weeks of age. Red line in the sagittal views indicates the plane shown in the axial view. Red arrowheads show ossification ligaments. Scale bars: 2000 μm (sagittal) and 1000 μm (axial). **B**, Representative images of H&E, toluidine blue, and double ALP-TRAP staining of sagittal sections of the full spine and of the ossified lesion in 8-week-old mice (magnification 4 \times or 10 \times). Arrows indicate osseous bridges in the H&E- and toluidine blue-stained lesion and epiphyseal plate chondrocytes and osteoblasts in the ALP-TRAP-stained lesion. Scale bar: 1000 μm in full-spine images; 200 μm in 4 \times magnification images. **C**, **D**, Magnified views show MSCs, marked by CD44 (green) and CD105 (red), around the ossified area of the posterior longitudinal ligament (PLL). *MSCs; #30 \times magnification. Scale bar: 200 μm in (C) and 50 μm in (D). ALP indicates alkaline phosphatase; H&E, hematoxylin and eosin; MSC, mesenchymal stem cell; WT, wild-type.

mice, with reactive hyperplasia in the annulus fibrosus cartilaginous cells. Bone trabeculae appeared in the center of the lesion at 8 weeks of age. Toluidine blue staining revealed lesions extending into the intervertebral discs. TRAP-ALP double staining identified epiphyseal plate chondrocytes and osteoblasts attached to the junction between the odontoid process and posterior longitudinal ligaments; these chondrocytes and osteoblasts were used to analyze the ossification state at 8 weeks of age (Figure 1B). Double immunofluorescence staining for the MSC markers CD44 and CD105 revealed double-positive MSCs surrounding the ossifying regions of the spinal ligaments (Figure 1C and D, asterisks). Thus, ligament ossification began during the 8th week, and MSCs may contribute to this ossification.

Sensory and Motor Dysfunction in *ttw* Mice

WT and *ttw* mice were assessed by BMS scores every 4 weeks (Figure 2A). The BMS score for the *ttw* mice dropped significantly below that of WT mice beginning at 12 weeks of age. Hindlimb sensitivity to heat and to cutaneous and mechanical stimuli was also assessed at 4-week intervals from 4 to

20 weeks of age. The mean reaction force to innocuous mechanical stimuli was significantly lower in *ttw* than in WT mice at 8, 12, and 16 weeks of age (Figure 2B). The reaction time to mechanical stimuli was significantly longer in *ttw* than in WT mice at 8 and 12 weeks of age (Figure 2C). The reaction time to noxious heat was significantly longer in WT than in *ttw* mice at 4 weeks of age. But reaction time to noxious heat was significantly longer in *ttw* than in WT mice at 8 and 16 weeks of age; it also increased significantly with age in the *ttw* mice, but not in WT mice (Figure 2D).

Immunophenotypic Characterization of Mesenchymal Stem Cell Markers

Flow cytometry showed that WT and *ttw* A-MSCs expressed CD105 (74.7% \pm 0.4% and 71.3% \pm 1.4%, respectively) but not CD34 (4.4% \pm 1.9%, 4.6% \pm 0.3%) or CD45 (2.3% \pm 0.6%, 2.1% \pm 0.1%) (Figure 3A and B). M-MSCs from WT and *ttw* mice also expressed CD105 (80% \pm 9.2%, 78% \pm 7.8%) but not CD34 (7.2% \pm 1.0%, 3.0% \pm 0.6%) or CD45 (3.6% \pm 1.0%, 3.6% \pm 0.6%) (Figure 3A and B). Thus, A-MSCs and M-

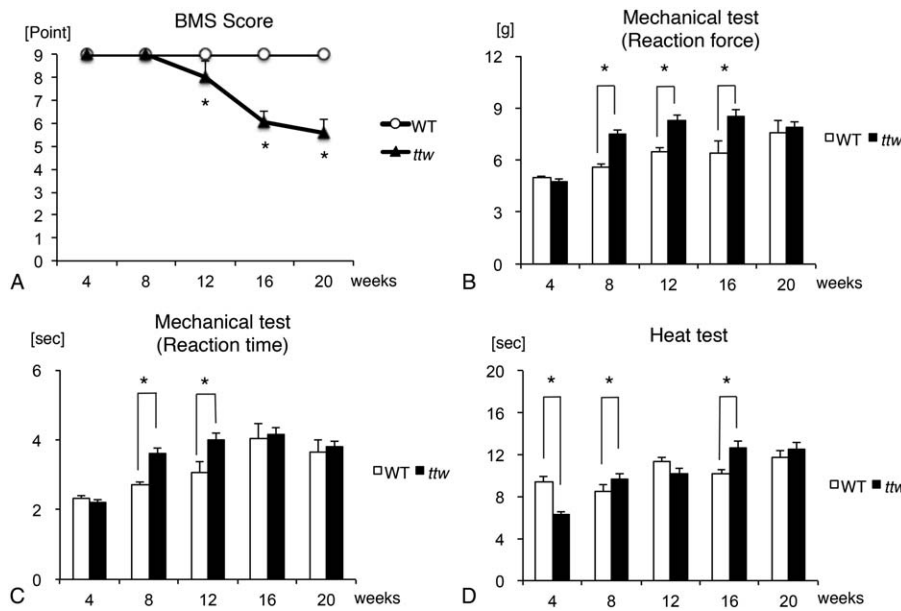


Figure 2. Analysis of motor and sensory dysfunction. **A**, Open-field walking ability as determined by BMS scores. Hindlimb function was scored from 0 to 9 (flaccid paralysis to normal gait). **B–D**, Mice were tested at 4-week intervals for hind-paw responses to innocuous mechanical (**B** and **C**) and heat (**D**) stimuli. $n=5$. Values are means \pm SE. $*P < 0.05$. BMS indicates Basso Mouse Scale; WT, wild-type.

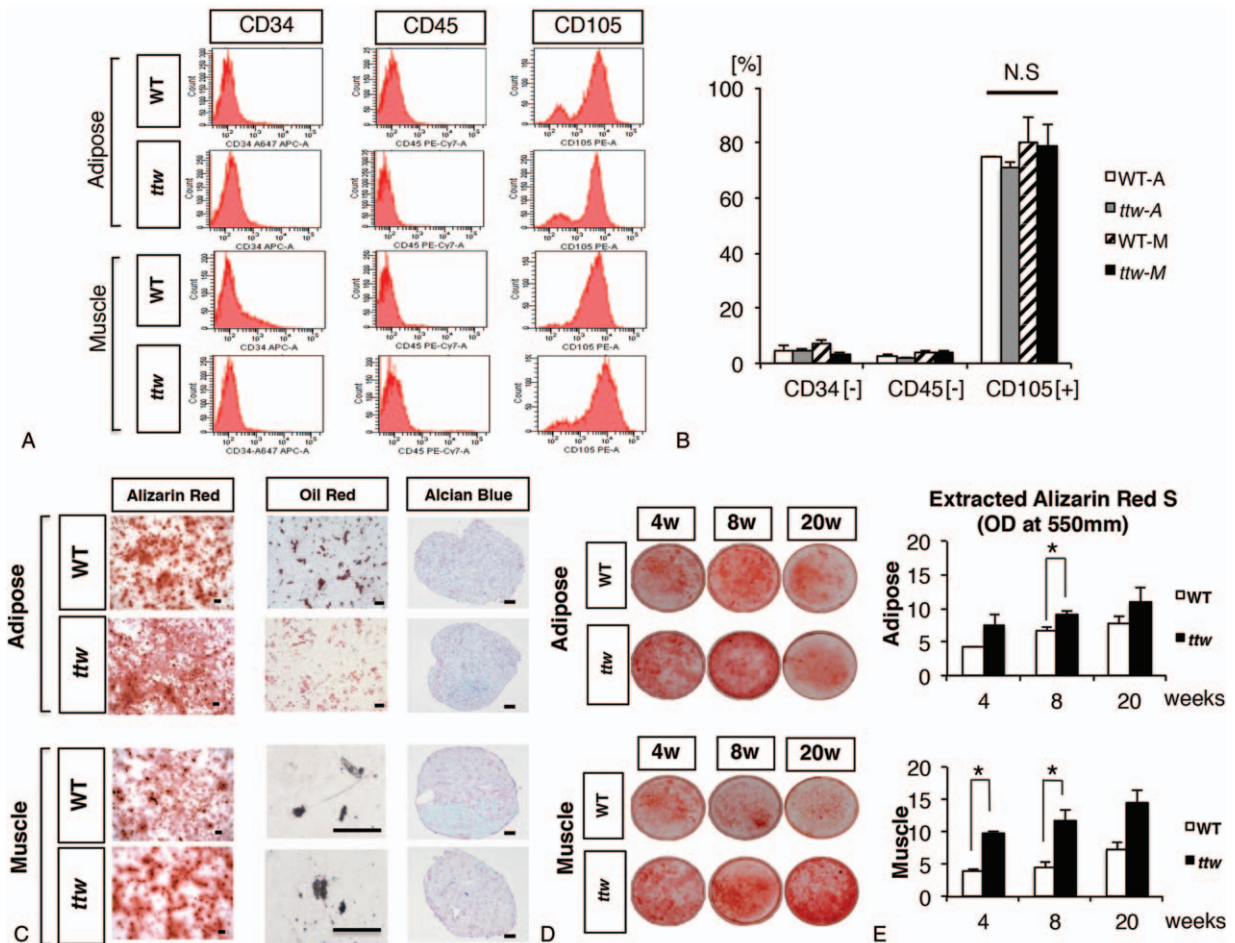


Figure 3. Mesenchymal stem cells (MSCs) from WT and *ttw* adipose and muscle tissues showed stem cell-specific surface markers and multilineage differentiation, and osteogenic differentiation potential in *ttw* MSCs. **A**, Histograms for each surface marker. **B**, Adipose and muscle MSCs from WT and *ttw* mice were positive for CD105 and negative for CD34 and CD45. A: adipose MSCs; M: muscle MSCs. **C**, Alizarin Red S-stained mineralization in osteogenesis; Oil Red O-stained lipid vacuoles in adipogenesis. Scale bar: 200 μ m. Sections were stained with Alcian Blue. Scale bar: 50 μ m. **D**, Osteogenic differentiation potential assessed by Alizarin Red S. **E**, Bound Alizarin Red S was dissolved and its absorbance measured at 550 nm to quantify mineral content ($n=3$). Values are means \pm SE. $*P < 0.05$. NS indicates no significant difference; WT, wild-type.

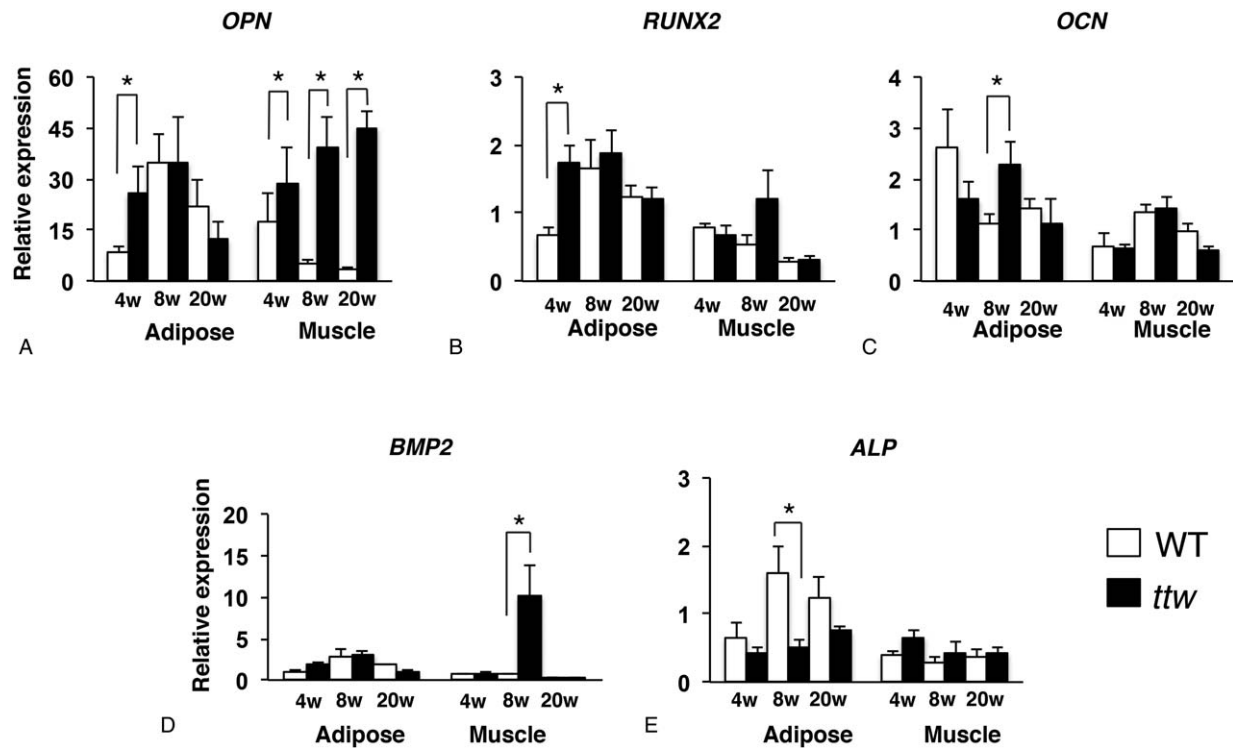


Figure 4. High osteogenic gene expression in *ttw* MSCs, RT-qPCR analysis of the osteogenic markers (A) osteopontin (*OPN*), (B) runt-related transcription factor 2 (*RUNX2*), (C) osteocalcin (*OCN*), (D) bone morphogenetic protein 2 (*BMP2*), and (E) alkaline phosphatase (*ALP*) in *ttw* and WT MSCs. *Significant difference ($n = 3$). Values are means \pm SE. * $P < 0.05$.

MSCs derived from *ttw* mice and WT mice had nearly identical characteristics, with no significant differences.

Multilineage and High Osteogenic Potentials of *ttw* Adipose-Derived Mesenchymal Stem Cells and Muscle-Derived Mesenchymal Stem Cells

To examine the multilineage potential of WT and *ttw* MSCs, A-MSCs and M-MSCs from WT and *ttw* mice were induced into osteocytes, adipocytes, and chondrocytes, which were stained by Alizarin Red, Oil Red O, and Alcian Blue, respectively. A-MSCs and M-MSCs derived from WT and *ttw* mice had nearly identical multilineage differentiation characteristics (Figure 3C), although the *ttw* A-MSCs and M-MSCs had significantly higher optical density values for Alizarin Red than the WT MSCs (Figure 3D and E).

High Osteogenic Gene Expression in Mesenchymal Stem Cells From *ttw* Mice

The expression of osteogenic genes was assessed by real-time (RT)-qPCR at 4, 8, and 20 weeks of age (Figure 4A–E). *OCN*, *OPN*, and *RUNX2* were expressed at significantly higher levels in *ttw* than in WT A-MSCs. *OPN* and *BMP2* were expressed at significantly higher levels in *ttw* than in WT M-MSCs. *ALP* was expressed more strongly in the WT group than in the *ttw* group.

DISCUSSION

This is the first time course study to assess A-MSC and M-MSC characteristics and sensory function in *ttw* mice over

an extended period. Sensory dysfunction began at 8 weeks of age in *ttw* mice and motor dysfunction at 12 weeks, indicating that sensory function was more sensitive to ligament ossification. MSCs derived from *ttw* muscle/adipose tissue had high osteogenic potentials. There was a correlation between the osteogenic potential of MSCs derived from 8-week-old *ttw* mice and ligament ossification.

Previous micro-CT studies of *ttw* mice found that ossified lesions begin to develop in the longitudinal ligament at 6 weeks of age, with severe spinal cord compression appearing on magnetic resonance imaging at about 20 weeks.^{22,23} Histological analysis showed that the ossification is newly produced at 6 weeks and enlarged at 22 weeks.^{24,25} Our micro-CT results showed that spinal ligaments began to ossify at 8 weeks, and that the ossified area continued to expand through the 20th week. Pathology confirmed the presence of new ossification at 8 weeks of age. We previously demonstrated that MSCs are present near the ossification front and might contribute to the ectopic ossification process of the flavum ligament through endochondral ossification. In the present study, immunohistochemical analysis showed that cells expressing the MSC markers CD44 and CD105 were present near the OPLL region, and around the ossifying region. These results suggest a correlation between MSCs and OPLL.

Behavioral analyses have shown a correlation between spinal compression and motor-function loss. Cervical cord compression may cause atrophy²⁶ and axonal disruption.²³ Humans with OPLL commonly complain of impaired sensory function.²⁷ The hyposensitivity observed in 8-week-old *ttw*

mice may have resulted from ossification-related compression of the cervical spinal cord. Sensory dysfunction appeared at 8 weeks, and motor dysfunction at 12 weeks of age.

We previously reported that MSCs from subjects with OPLL have higher osteogenic potential and express osteogenesis-related genes at higher levels than MSCs from subjects without OPLL. After 21 days of osteogenic induction, ALP expression in the MSCs from PLLs is comparable in human subjects with or without OPLL.¹² Adipose and muscle tissue, along with ligaments, are derived from the mesoderm-layer tissues.²⁸ Here we found that *ttw* A-MSCs and M-MSCs strongly expressed osteogenic genes except for ALP. Patients with OPLL strongly express ALP in PLL cells.²⁹ Our present RT-qPCR results indicated that both A-MSCs and M-MSCs tended toward the osteogenic lineage, and that A-MSCs and M-MSCs from 8-week-old *ttw* mice had a higher osteogenic potential than those from WT mice. Furthermore, these changes in osteogenic gene expression were correlated with the micro-CT, behavior (sensory function), and pathology results.

Our study has some limitations. The mechanism underlying the higher osteogenic potential of *ttw* mouse A-MSCs and M-MSCs remains unclear. Also, the WT and *ttw* mice were of different strains; the WT mice are a common inbred laboratory strain that presents reliable and stable research data as a control group. The *ttw* mice are a naturally occurring mutant mouse originating from the Institute of Cancer Research Japan strain. Finally, the ossification ligament tissue cannot be isolated cleanly from the narrow spinal cord in *ttw* mice; thus, we assessed MSCs from adipose and muscle tissue.

Our results suggest that sensory function was more sensitive than motor function to disruption from spinal ligament ossification. MSCs derived from *ttw* mice had a higher osteogenic potential than those from WT mice. These results reveal a correlation between the pathogenesis of spinal ligament ossification and the osteogenic potential of MSCs observed in *ttw* mice. In this regard, MSCs derived from *ttw* mice could be used *in vitro* to study the mechanism of MSCs in OPLL. Pharmaceutical experiments with *ttw* mice will also improve our understanding of OPLL.

➤ Key Points

- ❑ The osteogenic potential of A-MSCs and M-MSCs from *ttw* mice, a model of OPLL, was examined along with the disease pathogenesis.
- ❑ Micro-CT and histological and immunofluorescence staining revealed MSC-associated ligament ossification in the *ttw* mice starting at 8 weeks of age.
- ❑ The *ttw* mice became hyposensitive at 8 weeks of age and showed motor function deficits by 12 weeks of age, indicating that sensory function was more sensitive to ligament ossification than motor dysfunction.

- ❑ A-MSCs and M-MSCs from *ttw* mice had a higher osteogenic potential than WT MSCs, based on histological, biochemical, and RT-qPCR analyses.
- ❑ The high osteogenic potential of MSCs from *ttw* mice was correlated with ligament ossification and the loss of sensory function in these mice.

Acknowledgments

The authors thank CLEA Japan, Inc., Makoto Kajiwarra for technical assistance. The authors also thank Dr. Chikara Ohyama, Mr. Tohru Yoneyama, and Mr. Kenji Kabawasa of the Department of Urology, Hirosaki University Graduate School of Medicine, for excellent technical assistance with the flow cytometric analysis, and Mr. Kazuhiko Seya of the Department of Pharmacology, Hirosaki University Graduate School of Medicine for excellent technical assistance along with valuable advice and discussion.

References

1. Ehara S, Shimamura T, Nakamura R, et al. Paravertebral ligamentous ossification: DISH, OPLL and OLF. *Eur J Radiol* 1998; 27:196–205.
2. Inamasu J, Guiot BH, Sachs DC. Ossification of the posterior longitudinal ligament: an update on its biology epidemiology and natural history. *Neurosurgery* 2006;58:1027–38.
3. Furukawa K. Pharmacological aspect of ectopic ossification in spinal ligament tissues. *Pharmacol Ther* 2008;118:352–8.
4. Prockop DJ. Marrow stromal cells as stem cells for nonhematopoietic tissues. *Science* 1997;276:71–4.
5. Segawa Y, Muneta T, Makino H, et al. Mesenchymal stem cells derived from synovium, meniscus, anterior cruciate ligament, and articular chondrocytes share similar gene expression profiles. *J Orthop Res* 2009;27:435–41.
6. Red-Horse K, Ueno H, Weissman IL, et al. Coronary arteries form by developmental reprogramming of venous cells. *Nature* 2010; 464:549–53.
7. Nelson ER, Wong VW, Krebsbach PH, et al. Heterotopic ossification following burn injury: the role of stem cells. *J Burn Care Res* 2012;33:463–70.
8. Chen JH, Yip CY, Sone ED, et al. Identification and characterization of aortic valve mesenchymal progenitor cells with robust osteogenic calcification potential. *Am J Pathol* 2009;174:1109–19.
9. Davis TA, Lazdun Y, Potter BK, et al. Ectopic bone formation in severely combat-injured orthopedic patients—a hematopoietic niche. *Bone* 2013;56:119–26.
10. Asari T, Furukawa K, Tanaka S, et al. Mesenchymal stem cell isolation and characterization from human spinal ligaments. *Biochem Biophys Res Commun* 2012;417:1193–9.
11. Chin S, Furukawa K, Ono A, et al. Immunohistochemical localization of mesenchymal stem cells in ossified human spinal ligaments. *Biochem Biophys Res Commun* 2013;436:698–704.
12. Harada Y, Furukawa K, Asari T, et al. Osteogenic lineage commitment of mesenchymal stem cells from patients with ossification of the posterior longitudinal ligament. *Biochem Biophys Res Commun* 2014;443:1014–20.
13. Hosoda Y, Yoshimura Y, Higaki S. A new breed of mouse showing multiple osteochondral lesions—*twy* mouse. *Ryumachi* 1981;21 (suppl):157–64.
14. Takano M, Kawabata S, Komaki Y, et al. Inflammatory cascades mediate synapse elimination in spinal cord compression. *J Neuroinflammation* 2014;11:40.
15. Kumagai G, Tsoulfas P, Toh S, et al. Genetically modified mesenchymal stem cells (MSCs) promote axonal regeneration and prevent hypersensitivity after spinal cord injury. *Exp Neurol* 2013; 248:369–80.

16. Basso DM, Fisher LC, Anderson AJ, et al. Basso Mouse Scale for locomotion detects differences in recovery after spinal cord injury in five common mouse strains. *J Neurotrauma* 2006;23:635–59.
17. Chaplan SR, Bach FW, Pogrel JW, et al. Quantitative assessment of tactile allodynia in the rat paw. *J Neurosci Methods* 1994;53:55–63.
18. Hargreaves K, Dubner R, Brown F, et al. A new and sensitive method for measuring thermal nociception in cutaneous hyperalgesia. *Pain* 1988;32:77–88.
19. Yamamoto N, Akamatsu H, Hasegawa S, et al. Isolation of multipotent stem cells from mouse adipose tissue. *J Dermatol Sci* 2007;48:43–52.
20. Sung JH, Yang HM, Park JB, et al. Isolation and characterization of mouse mesenchymal stem cells. *Transplant Proc* 2008;40:2649–54.
21. Gregory CA, Gunn WG, Peister A, et al. An alizarin red-based assay of mineralization by adherent cells in culture: comparison with cetylpyridinium chloride extraction. *Anal Biochem* 2004;329:77–84.
22. Wang J, Wang X, Rong W, et al. Alteration in chondroitin sulfate proteoglycan expression at the epicenter of spinal cord is associated with the loss of behavioral function in Tiptoe walking Yoshimura mice. *Neurochem Res* 2014;39:2394–406.
23. Takano M, Komaki Y, Hikishima K, et al. In vivo tracing of neural tracts in tiptoe walking Yoshimura mice by diffusion tensor tractography. *Spine (Phila Pa 1976)* 2013;38:E66–72.
24. Uchida K, Nakajima H, Watanabe S, et al. Apoptosis of neurons and oligodendrocytes in the spinal cord of spinal hyperostotic mouse (twy/twy): possible pathomechanism of human cervical compressive myelopathy. *Eur Spine J* 2012;21:490–7.
25. Uchida K, Yayama T, Sugita D, et al. Initiation and progression of ossification of the posterior longitudinal ligament of the cervical spine in the hereditary spinal hyperostotic mouse (twy/twy). *Eur Spine J* 2012;21:149–55.
26. Baba H, Maezawa Y, Imura S, et al. Quantitative analysis of the spinal cord motoneuron under chronic compression: an experimental observation in the mouse. *J Neurol* 1996;243:109–16.
27. Yonenobu K, Nakamura Y, Toyama. OPLL: Ossification of the Posterior Longitudinal Ligament ed. Springer, 2006.
28. Yusuf F, Brand-Saberi B. The eventful somite: patterning, fate determination and cell division in the somite. *Anat Embryol* 2006;211 (suppl 1):21–30.
29. Ishida Y, Kawai S. Characterization of cultured cells derived from ossification of the posterior longitudinal ligament of the spine. *Bone* 1993;14:85–91.